PHOTONICS **Research**

Rectangular single-mode polymer optical fiber for femtosecond laser inscription of FBGs

Jitendra Narayan Dash, Xin Cheng,* Dinusha Serandi Gunawardena, and Hwa-Yaw Tam

Photonics Research Centre, Department of Electrical Engineering, The Hong Kong Polytechnic University, Kowloon, Hong Kong, China
Corresponding author: eechengx@polyu.edu.hk

In this study, a novel rectangular polymer single-mode optical fiber for femtosecond (fs) laser-inscribed fiber Bragg gratings (FBGs) is proposed and demonstrated. The cylindrical geometry of the widely used circular fiber elongates the fs laser beam along the fiber axis, resulting in reduced laser intensity and requiring index-matching oil immersion during FBG inscription. However, the flat geometry and negligible surface roughness of the featured fiber significantly diminish this lensing distortion and eliminate the need for oil immersion, thereby resulting in optimal focusing of the laser beam, permitting direct and efficient inscription of FBGs within the optical fiber. The core and cladding of the rectangular fiber were fabricated using two different grades of ZEONEX, a cyclo olefin polymer, which have slightly different refractive indices. The similar glass transition temperature for core and cladding simplifies the fiber drawing process, and a rectangular single-mode optical fiber with dimensions of 213 μm × 160 μm and core diameter of 9.4 μm was fabricated using an in-house fiber drawing facility. A second harmonic (520 nm) fs laser beam was used to successfully inscribe a 2-mm-long FBG in the rectangular fiber within a few seconds with a point-by-point technique. The inscription of a single FBG leads to the excitation of higher order FBG peaks at 866.8 and 1511.3 nm, corresponding to widely used wavelength bands in fiber optic sensing. The strain and temperature sensitivities of the FBG were measured to be 7.31 nm/%ε (0.731 pm/με) and 10 pm/°C, and 12.95 nm/%ε (1.29 pm/με) and 15 pm/°C at 866.8 nm and 1511.3 nm, respectively.   © 2021 Chinese Laser Press

https://doi.org/10.1364/PRJ.434252

1. INTRODUCTION

Femtosecond (fs) lasers offer an exciting new technology that permits the fabrication of various kinds of novel optical devices in optical fibers, including gratings, optical waveguides, miniature sensors, and interferometers [1–3]. The attraction of the fs laser based grating is driven by its unique advantages such as grating inscription without a phase mask and ability to inscribe gratings in any type of optical fiber including non-photosensitive fibers and different patterns of grating pitch [4]. In addition, the short duration of the pulses enables one to precisely control the spatial dimension of the refractive index (RI) modulation region in optical fiber [5]. Owing to the above advantages, fs laser based gratings have been inscribed in a wide variety of silica based fibers for various sensing applications [6–8]. Although, a silica based fiber Bragg grating (FBG) can be used to measure various physical parameters, its high Young's modulus (~70 GPa) limits its sensitivity and applicability in applications that require measurements to be conducted in constricted spaces with small bending radii and under certain conditions that require fibers to successfully withstand high strains without breakage. On the other hand, polymer optical fibers (POFs), owing to their unique physical and mechanical properties such as larger elastic strain limit, low Young's modulus, low brittleness, enhanced bending tolerance, and biocompatibility, have considerable advantages over their silica counterparts [9–11]. Over the past few years, substantial progress has been made in the fabrication of POF based gratings for sensing applications [12–21]. For example, both pulsed and continuous lasers have been utilized for the inscription of gratings in doped PMMA fibers [13,14,22–24]. However, the range of applications is limited due to their high optical absorption around 1550 nm introduced by the dopants, and considerably strong affinity to water. In addition, fibers based on polycarbonate (PC) with high glass transition temperature and flexibility have been used in strain and humidity sensing applications [25,26]. POFs based on chemically inert and humidity insensitive cyclic olefin copolymers (COCs) such as TOPAS [15,27,28], cyclic olefin polymers (COPs) such as ZEONEX [11,29–31], and amorphous fluoropolymer such as CYTOP have also been demonstrated for sensing applications [16]. FBGs have been successfully inscribed in commercially available multimode CYTOP optical fibers using a fs laser

[32]. However, a single-mode optical fiber based on CYTOP is not commercially available. Previously, we successfully fabricated single-mode optical fibers using CYTOP (RI = 1.355) as the core and PMMA (RI = 1.45) as the cladding materials, and the measured attenuation of the fiber was ~0.2 dB/m at 1560 nm [33]. However, the layer of air between the core and cladding for guidance of light prevents FBG inscription in this type of fiber. Polymer single-mode optical fibers based on all ZEONEX or a combination of ZEONEX and TOPAS without the use of any dopants have been fabricated, and these fibers have been used for strain and temperature measurements [10,11,34], while a combination of ZEONEX and polysulfone (PSU) has been used for ultrahigh temperature measurements [31]. However, ZEONEX is preferable for strain sensing applications due to its lower Young's modulus (~2.2 GPa) as well as comparatively lower transmission loss than TOPAS, while its moisture absorption is much lower (55 times smaller) than that of PMMA [35]. Furthermore, the similar glass transition temperature of the core and cladding in ZEONEX fiber makes the fiber drawing process much easier compared to that of doped-core POFs, which are vulnerable to dopant diffusion [11,21]. In addition, long-term stability of FBGs fabricated in ZEONEX POFs was demonstrated based on a batch of ZEONEX POFs fabricated in 2019 and stored at room temperature over a year [10]. However, the high optical loss of ZEONEX at a 1550-nm transmission window restricts its usage to around 10 cm. On the contrary, in an 850-nm window, the loss is much lower, and this is adequate for most medical applications where the required fiber length is typically less than 2 m [11]. Therefore, shifting the operational wavelength to this window is a logical progression. Furthermore, commercial FBG interrogators are available for operation around 850 nm.

Recently, fs lasers have been utilized in the fabrication of FBGs in PMMA and CYTOP multi-mode fibers [9,19,31, 35–37]. Point-by-point (PbP) and line-by-line (LBL) inscription techniques demonstrated in these studies eliminate the need for phase masks. It is to be noted that the phase mask technique is useful for repeatable inscription of FBGs at specific wavelengths, while the PbP technique permits tailoring of the Bragg wavelength for FBG inscription at different orders or different wavelengths depending on the requirement of the sensing application. However, the focused fs laser beam experiences distortion effects when passing through a circular fiber that acts as a cylindrical lens. The lensing effect causes the laser beam to be more elongated as it moves towards the fiber core, which reduces laser intensity. The distortion also makes visualization of the fiber rather difficult. The lensing distortions can be diminished by immersing the optical fiber in index-matching (IM) oil and sandwiching it between two thin glass slides. Alternatively, a section of fiber can be polished down to a D shape to avoid the cylindrical lensing effect. However, polishing reduces the mechanical strength; for large scale production of sensing probes, each section of the fiber needs to be polished down to a D shape, and the polishing parameters have to be controlled precisely for reproducibility, which is highly time consuming.

In this paper, we propose a novel rectangular POF to diminish the lensing distortion, thereby avoiding the use of IM oil

during FBG inscription using the fs laser. The main challenge is designing and fabricating a rectangular fiber with flat surfaces since a small variation in the writing plane (≤1 μm) during grating inscription results in a significant change in the spectral response of the FBG. The PbP technique can be used to excite specific higher order FBG peaks, which correspond to the widely used wavelength bands for sensing applications. Additionally, the unique material properties of ZEONEX coupled with the rectangular geometry and lack of IM oil immersion further enhance the distinctive advantages. These features could open up the potential for many applications. Furthermore, the larger contact area of the rectangular fiber compared to that of a circular optical fiber provides better strain transfer to a surface attached FBG [38,39]. Additionally, due to the presence of a flat surface on each side, the rectangular fiber is easy to fix on the flat surface of the glass plate for inscription of FBG compared to that of a D-shaped fiber whose flat surface needs to be adjusted properly with respect to the incident laser beam.

2. RECTANGULAR OPTICAL FIBER FABRICATION AND FLATNESS CHARACTERIZATION

A. Fabrication of ZEONEX Rectangular Optical Fiber

The rectangular optical fiber preform was fabricated using the pull through method [10]. The core and cladding of the fiber were made of different grades of ZEONEX, namely, ZEONEX E48R and ZEONEX 480R, respectively [10,11,31]. The RI of E48R is 1.531 (at ~600 nm), which is slightly higher than that of 480R (1.525). The step-by-step preform fabrication process is shown in Fig. 1. It involves three stages: (1) fabrication of the cladding preform with a central hole as shown in Figs. 1(a)–1(c), (2) fabrication of the core preform, shown in Figs. 1(d) and 1(e), and (3) drawing of the core preform into
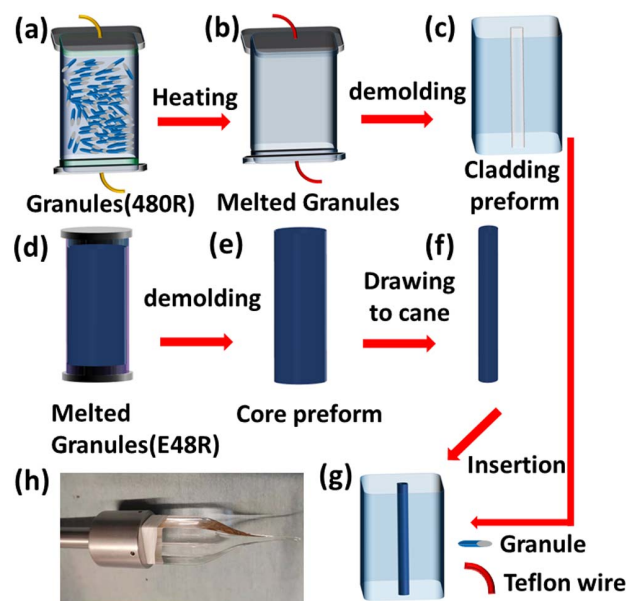

Fig. 1. (a)–(g) Fabrication procedure of ZEONEX based rectangular polymer optical fiber preform and (h) image of the rectangular preform after a segment of it was drawn into rectangular optical fiber.

a cane and insertion of the cane into the cladding preform, as shown in Figs. 1(f) and 1(g). A rectangular quartz tube as shown in Fig. 1(a), sealed with Teflon caps at both ends, was used to fabricate the preform for the cladding. The Teflon caps have a central hole with 1 mm diameter, and a Teflon wire (diameter = 0.9 mm) was threaded through the holes of the two Teflon caps. The rectangular quartz tube was filled with ZEONEX 480R granules and heated at 245° C in a vacuum oven for 20 h, and then the tube was slowly cooled down to room temperature over 10 h. Afterwards, the Teflon wire was removed from the cladding preform, leaving behind a central hole as shown in Fig. 1(c). A cylindrical glass tube filled with ZEONEX E48R granules was heated and cooled under the same conditions as described above to make the core preform shown in Figs. 1(d) and 1(e), respectively. The core preform was then drawn into a cane [shown in Fig. 1(f)] of 0.9 mm diameter using the in-house fiber drawing tower. The cane was inserted into the central hole of the cladding preform [shown in Fig. 1(g)], and the complete preform was annealed at 120°C for 10 h to remove any residual moisture. The complete preform was then drawn into a rectangular fiber. The remaining section of the preform after the fiber drawing process is shown in Fig. 1(h). Figure 2(a) shows the cross section of the rectangular fiber with the fiber core illuminated with white light. As can be seen from the figure, the core is circular while the cladding is rectangular. The dimensions of the rectangular fiber cross section are 213 μm × 160 μm, and the diameter of the core is 9.4 μm. The simulated profile of the core mode is shown in Fig. 2(b). The mode field diameter has been calculated to be 10.06 μm using the Petermann II equation [40], which is similar to the mode field diameter of a standard single-mode optical fiber (10.4 μm at 1550 nm). The transmission loss of the fiber was measured by a cut back method and found to be 8.5 dB/m at 855 nm, which is higher compared to the previously reported 3.02 dB/m [11]. Optimization of preform fabrication and fiber drawing conditions is vital in reducing the loss of the fiber.

B. Surface Flatness Characterization

The surface of the rectangular optical fiber through which the fs laser beam is focused onto the core must be extremely flat to avoid any distortion of the laser beam. This is because a small change in the flatness of the writing plane (x–z plane as shown in Fig. 3) during FBG fabrication may affect the FBG spectrum. A second harmonic beam from the fs laser (Spectra-Physics Spirit One) at an emission wavelength of 520 nm with a repetition rate of 100 Hz and a pulse duration of 250 fs was
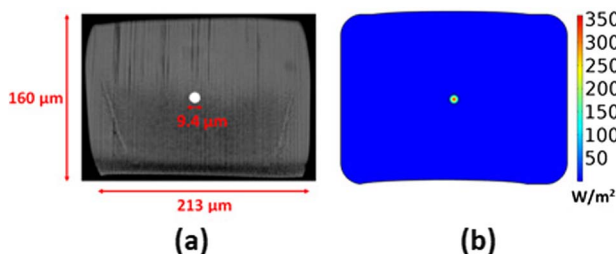

Fig. 2. (a) Cross section of the ZEONEX rectangular optical fiber with light guidance through the core and (b) simulated profile of the core mode.
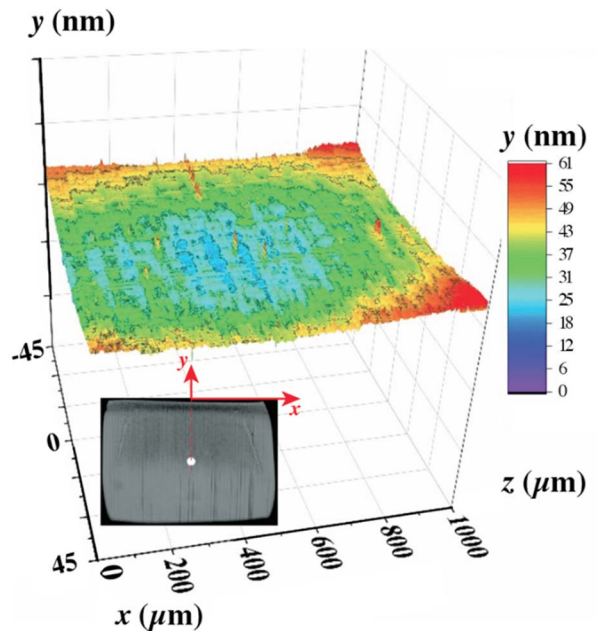

Fig. 3. 3D surface profile measurement result of the ZEONEX rectangular optical fiber.

used in the FBG fabrication process. A 40× objective lens (Zeiss) with an NA of 0.75 was used to focus the laser beam, which has superior beam quality (TEM$_{00}$, $M^2 < 1.2$). The $1/e^2$ radius of the incident laser beam on the fiber surface is about 20 μm. Therefore, it is crucial that the surface above the core is flat and its roughness is less than the wavelength of the incident laser beam over a length of 2 mm and a width of 90 μm (Fig. 3) to diminish any distortion in the focused fs laser beam during the fabrication of a 2-mm-long FBG.

A laser scanning confocal microscope capable of measuring surface roughness with nanometer resolution (Keyence's VK-X200) was used to conduct an area scan of the fiber surface. The surface of the rectangular optical fiber was sputter coated with a 25-nm layer of gold to increase the contrast of the measurement. Figure 3 shows the 3D measurement results of the fiber surface covering ±45 μm in the x direction and 1 mm in the z direction, which is limited by the 1-mm measurement range of the equipment. The flatness in this region is better than 0.1 μm, which is adequate for inscription of good quality FBGs in the fiber without the need for IM oil. Similar reflection spectral profiles obtained for 2-mm-long FBGs inscribed at various sections of the optical fiber verify that the surface roughness of the fiber is suitable for writing 2-mm-long FBGs.

3. RESULTS AND DISCUSSION

A. FBG Inscription Process and Focusing of Laser Beam onto Circular and Rectangular Fibers

The laser beam passed through a half-wave plate followed by a Glan laser polarizer, collimator, and quarter-wave plate and then was reflected from a dichroic mirror before being focused onto the fiber. The reflected beam was then focused onto the fiber by a 40× microscope objective lens, and the energy of the laser was fixed at ~20 nJ. The repetition rate of the laser can be

controlled using a pulse picker divider where it was set to 100 Hz during the grating writing process. The velocity of the stage was precisely controlled to obtain the desired pitch of the grating, which was fixed at 2 μm for the proposed fiber. The fiber was placed on a glass slide and fixed on two ends. The glass slide was in turn mounted onto a high precision three-axis translational stage (Newport, XMS100-S for x and y axes with resolution of 0.05 μm and XMS50-S for z axis with resolution <1 nm), where the scanning direction was along the z direction of the fiber (see inset of Fig. 3). The fiber was illuminated with the aid of an LED, and the reflected light passing through a subsequent dichroic mirror was collected at a CCD, thereby, enabling real-time monitoring of the FBG inscription process. The synchronization of the laser beam and the three-axis translation stage was utilized to carry out FBG inscription in these fibers using the PbP technique. After grating inscription, the fiber was annealed at 80°C for 24 h to remove any residual stress of the fiber.

Prior to FBG inscription, investigations were carried out to ensure optimal focusing of the laser beam onto circular and rectangular optical fibers. In addition, the effect of incorporating IM oil was explored as well. When the laser beam is focused onto the circular fiber in the absence of IM oil, a focal mismatch occurs (astigmatism) between the axial (parallel to the fiber axis) [see Fig. 4(a)] and radial (perpendicular to the fiber axis) [see Fig. 4(b)] parts of the laser beam. In other words, when the radial beam is focused onto the core, the axial beam is focused outside the core. Due to the cylindrical geometry of the fiber, optical confinement of light at the radially focused region is higher compared to that of the axial beam resulting in a higher laser induced RI modification in the former. When both these effects are taken into consideration simultaneously, the region of inscription in the fiber core will be axially elongated as shown in Fig. 4(a). The microscope image of the elongated laser beam induced inscription region is shown in Fig. 4(c). However, in the presence of IM oil, the error introduced by curvature is eliminated and both parts of the beam, axial and radial, are focused onto a single point.
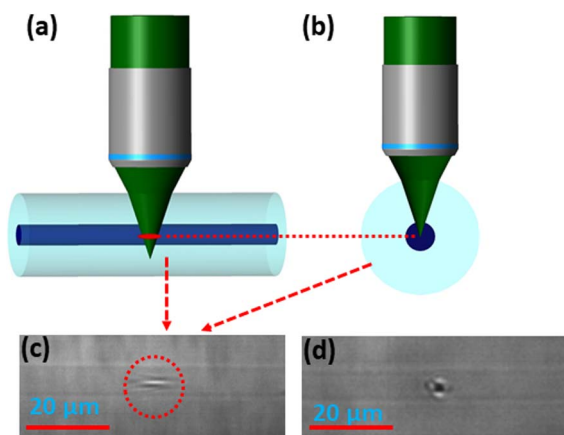

Fig. 4. Schematic illustrations of (a) axial (side view) and (b) radial (cross sectional view) aspects of the focused laser beam onto a circular fiber without IM oil. The red region in (a) indicates the elongated focal region. Microscope images of fs laser inscribed regions in circular fiber in (c) the absence and (d) presence of IM oil.
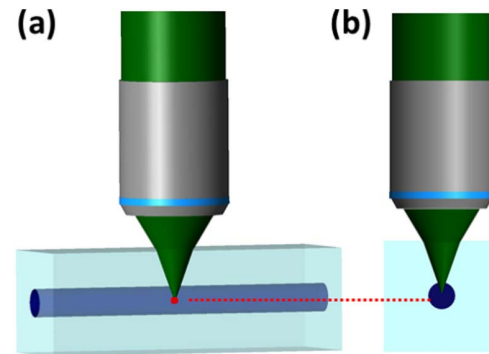

Fig. 5. Schematic illustrations of (a) axial (side view) and (b) radial (cross sectional view) parts of focused laser beam onto the rectangular fiber without IM oil.
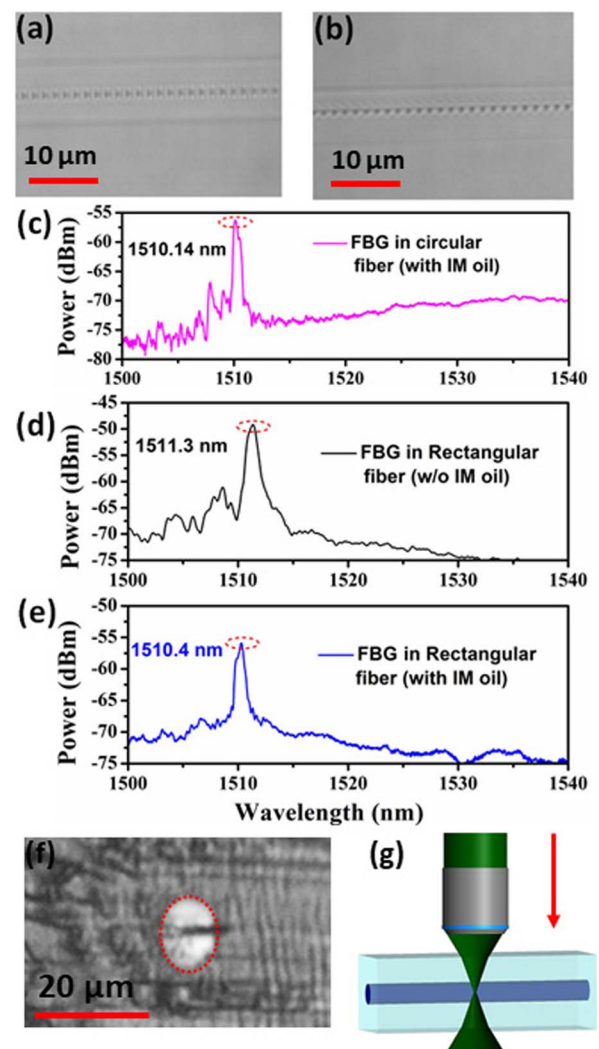

Fig. 6. Microscope images of FBGs inscribed in ZEONEX rectangular fiber (a) without and (b) with IM oil. Reflection spectra of the inscribed FBGs (c) with IM oil in circular fiber, (d) without and (e) with IM oil in rectangular fiber. (f) Cross sectional view of the grating in (a), where the red dashed circle refers to the core and the black line refers to the laser irradiated region. (g) Schematic illustration of the focused laser beam in Gaussian form, and the red arrow shows the beam direction.

The corresponding microscope image is shown in Fig. 4(d). On the contrary, there is no focal mismatch between the axial and radial parts of the laser beam due to the flat surface of the rectangular fiber as shown in Figs. 5(a) and 5(b), respectively. Therefore, this leads to the formation of a point focal region as shown in Fig. 5(a). It should be noted that there is a possibility of an intensity reduction of the laser beam due to the surface roughness at the core–cladding interface. To further evaluate the degree of focus of the laser beam on the rectangular fiber, FBGs were inscribed in this fiber in the absence and presence of IM oil as shown in Figs. 6(a) and 6(b), respectively. The lower contrast and slight deviation from a point shape in Fig. 6(a) may be attributed to the negligible nonuniformity of the flat surface of the rectangular fiber. The spectra corresponding to the FBG inscribed in a circular fiber with oil and in a rectangular fiber without and with oil are shown in Figs. 6(c)–6(e). Figure 6(f) illustrates the cross section of a segment of the grating shown in Fig. 6(a). It can be clearly seen that the damage region extends from the fiber core to a part of the cladding, and the irradiated region has a rectangular shape of which the length and width were found to be 9.66 μm and 1.44 μm, respectively. This type of elongated spot arises due to the Gaussian nature of the focused beam as shown in Fig. 6(g).

B. Characterization of FBGs

Initially, the FBG was inscribed in a ZEONEX based rectangular fiber with the aid of a 248-nm excimer laser (Bragg Star) and a phase mask (Ibsen, 1027.6 nm). A 2-mm-long grating was inscribed in these fibers with two pulses, each having a pulse energy of 65 mJ and pulse duration of 25 ns. A broadband supercontinuum light source (YSL Photonics) was used to couple light to the FBGs inscribed in the rectangular fibers, and the corresponding reflection spectra are shown in Fig. 7. It is apparent from the figure that the reflection spectrum of the FBG has only a single peak at 1555.9 nm (effective index ~1.5164) in the 1500–1600 nm wavelength window, corresponding to a first order grating with no other visible peak in the 800–900 nm wavelength range. In contrast, FBG inscription using a fs laser with the aid of the PbP technique (pitch = 2 μm), led to the excitation of multiple peaks, corresponding to higher orders as shown in Fig. 8. As can be seen
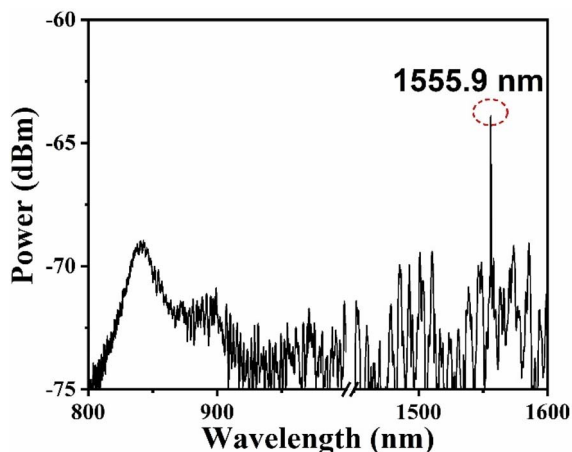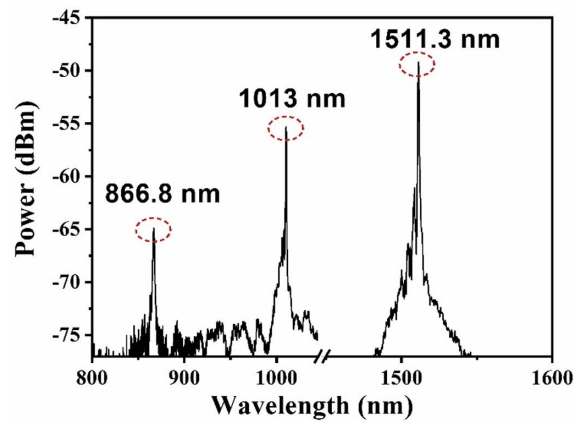
Fig. 8. Reflection spectrum of the FBG inscribed in ZEONEX rectangular fiber using fs laser exhibiting peaks at 866.8, 1013, and 1511.3 nm.

from the figure, an FBG with a peak at 1511.3 nm (effective index ~1.5120) is obtained in the 1500–1600 nm window, while the other two FBG peaks are obtained at 866.8 and 1013 nm. It should be noted that the pitch of the grating was fixed at 2 μm to achieve an FBG peak in the 850–880 nm wavelength window where ZEONEX based POF exhibits a low attenuation of less than 5 dB/m [11]. Although an FBG peak at a shorter wavelength (850–860 nm) can be obtained by tuning the pitch of the grating, the resultant spectra will not exhibit any peaks in the 1500–1600 nm wavelength range. Therefore, FBGs inscribed in the proposed fiber help in achieving two FBG peaks simultaneously at different wavelengths, where one corresponds to a region of low transmission loss, and the other is useful for sensing applications in the near IR region. Furthermore, this process avoids the need to inscribe FBGs separately at different wavelengths, thereby significantly reducing the inscription time. However, this type of probe can be utilized as a single point based sensing probe and, a quasi-distributed sensing array can be inscribed for applications requiring multi-point sensing. It should be noted that to achieve higher order peaks simultaneously using the phase mask technique, a customized phase mask of a specific pitch is required.

Afterwards, the strain and temperature responses of the FBGs inscribed using the aforementioned procedure were investigated. A segment of the ZEONEX rectangular fiber inscribed with an FBG was butt coupled to a silica fiber. The two ends of the FBG in the rectangular fiber were fixed onto two translational stages (MAX350/M, Thorlabs) as shown in Fig. 9. The distance between the glue point and the FBG was fixed at 1 cm. One of the stages was kept stationary while the other (1-μm resolution) was moved away from the FBG for application of strain. Light from a broadband supercontinuum source (YSL Photonics) was coupled to the FBG using an optical coupler, and the reflected light was analyzed using an optical spectrum analyzer (OSA, AQ6370D, Yokogawa, resolution = 0.02 nm). The peaks corresponding to 866.8 and 1511.3 nm can be simultaneously monitored using an OSA, although different interrogators can be used for each wavelength depending on the application. The strain introduced
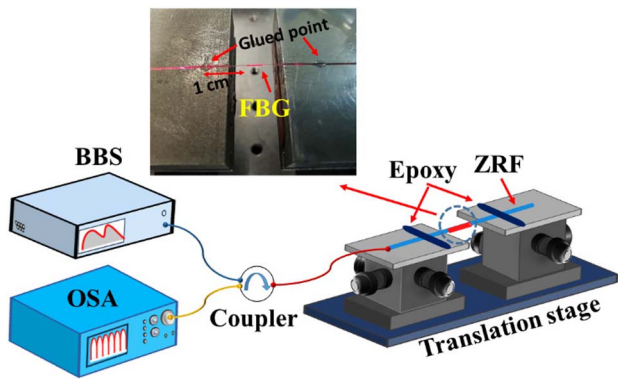
Fig. 7. Reflection spectrum of the FBG inscribed in ZEONEX rectangular fiber using 248-nm UV laser and phase mask technique.

Fig. 9. Experimental setup for strain measurement. Inset shows the FBG under investigation and the glued localities of the fiber. ZRF, ZEONEX based rectangular fiber; BBS, broadband source.

to the fiber was increased from 0% to 1% and then decreased from 1% to 0%, and this process was repeated for three cycles. The spectral response of the FBG peak (1511.3 nm) to the applied strain is shown in Fig. 10(a), and the shift in the FBG peak wavelength for three cycles is shown in Fig. 10(b). The average strain sensitivity after three cycles of measurement was found to be 12.95 nm/%ε (1.29 pm/με).

Fig. 10. (a) Spectral shift of the FBG peak (1511.3 nm) with applied strain. (b) Wavelength shift of the FBG peak with increasing and decreasing strain for three cycles of measurement with 1% change in strain for each cycle.
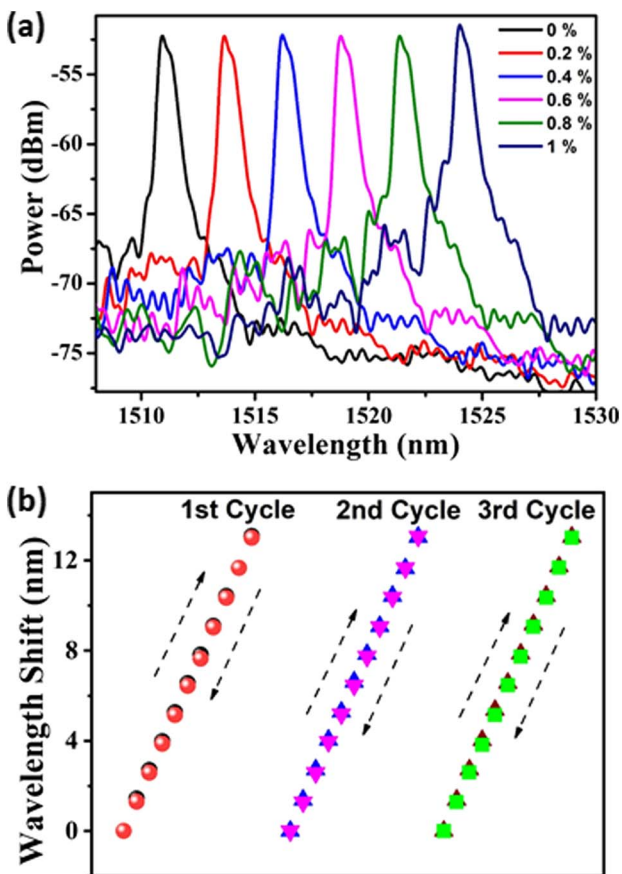

Fig. 11. (a) Spectral shift of the FBG peak (866.8 nm) with applied strain. (b) Wavelength shift of the FBG peak with increasing and decreasing strain for three cycles of measurement with 1% change in strain for each cycle.
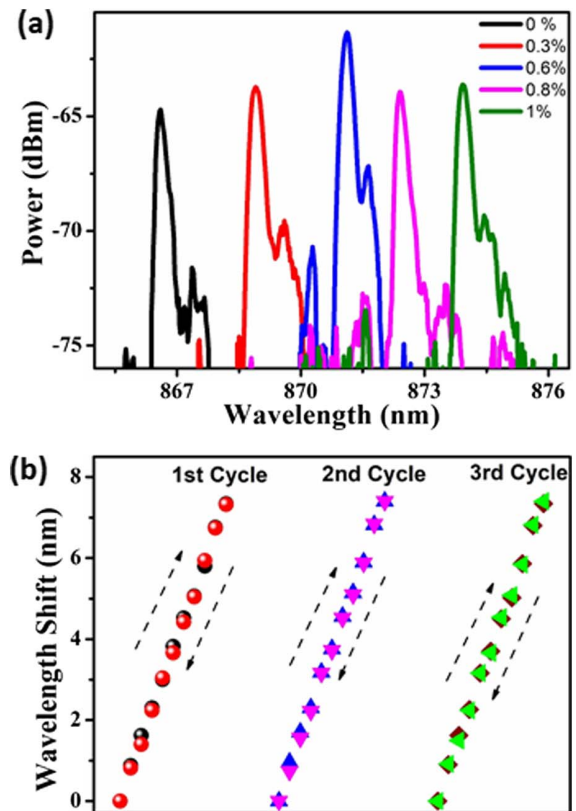
Following the same procedure, the spectral response of the FBG peak corresponding to 866.8 nm is plotted in Fig. 11(a), and the shift in FBG peak wavelength for three cycles of measurement is shown in Fig. 11(b). The average strain sensitivity in this scenario was found to be 7.31 nm/%ε (0.731 pm/με). Table 1 shows the strain response of the proposed probe along with other previously reported results.

The temperature responses of the FBG peaks corresponding to 866.8 and 1511.3 nm were analyzed by placing the sensor inside a tube furnace. The temperature was increased

Table 1. Comparison of Strain and Temperature Responses of POFBGs

| Type of Polymer	Strain Sensitivity	Temperature Sensitivity
TOPAS [15]	0.64 pm/με at ~868 nm	−78 pm/°C
CYTOP [16]	0.533 pm/με at ~600 nm	11.2 pm/°C
PMMA [24]	0.710 pm/με at ~841 nm	−54.50 pm/°C
PC [25]	0.701 pm/με at ~875 nm	−29.99 pm/°C
ZEONEX [11]	0.733 pm/με at ~855 nm	−9.78 pm/°C
ZEONEX [10]	1.6 pm/με at ~1553 nm	−24.7 pm/°C
ZEONEX mPOF [29]	0.77 pm/με at ~831 nm	−24.01 pm/°C
This work (ZEONEX)	0.731 pm/με at ~866 nm	−10 pm/°C
	1.29 pm/με at ~1511 nm	−15 pm/°C
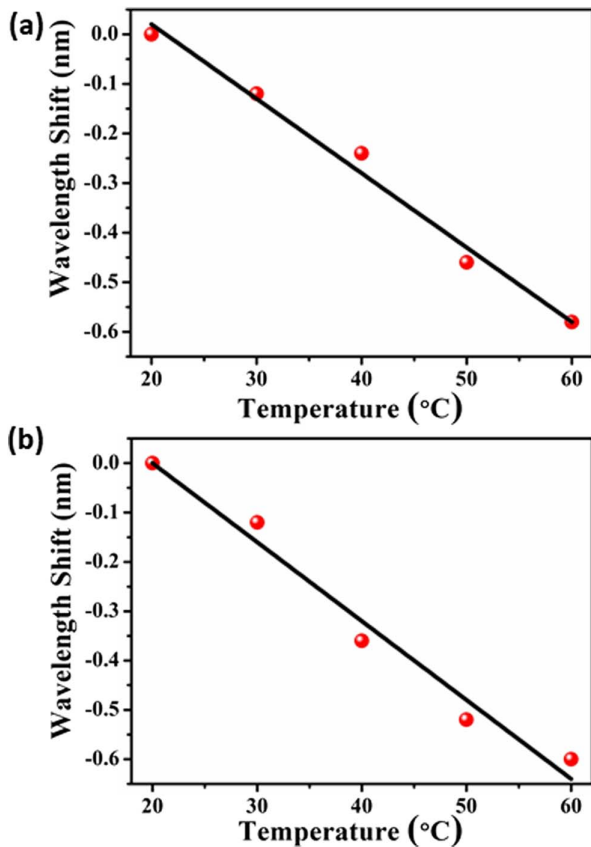
Fig. 12. Wavelength shift of the FBG corresponding to peaks at (a) 1511.3 nm and (b) 866.8 nm with increasing temperature.

from 20°C to 60°C in intervals of 10°C. The linear temperature responses of the FBG are shown in Figs. 12(a) and 12(b). The temperature sensitivity of the peak corresponding to 866.8 nm was found to be 10 pm/°C, while that corresponding to 1511.3 nm peak was found to be 15 pm/°C. Table 1 shows the temperature response of the proposed probe along with other previously reported results.

4. CONCLUSION

We have demonstrated fs laser inscribed FBGs in a novel rectangular shaped single-mode POF in which the core and cladding were composed of different grades of ZEONEX that ensured the fiber to be dopant free. The rectangular fiber with a good surface profile was drawn using the in-house fiber drawing facility. In contrast to their circular counterparts, the flat surface and the geometry of the rectangular fiber aid in the inscription of FBGs using the PbP technique without the requirement for IM oil, thereby significantly reducing the FBG inscription time, which greatly benefits mass production of FBGs. Fabrication of a single FBG led to the excitation of three different FBG peaks corresponding to different orders over the wavelength range from 800 to 1600 nm, out of which one was at 866.8 nm, where the transmission loss for ZEONEX is less, and the other was at 1511.4 nm. This process avoids the necessity for inscription of two individual gratings for different wavelengths, thereby once again contributing to a reduced FBG

inscription time. The strain and temperature responses of the grating were also analyzed, and the sensitivities were found to be 12.95 nm/%ε (1.29 pm/με) and 15 pm/°C at 1511.3 nm and 7.31 nm/%ε (0.731 pm/με) and 10 pm/°C at 866.8 nm, respectively. Hence, the fabrication of the flat rectangular fiber along with the inscription of a single FBG for two important wavelength bands opens up the possibility for efficient and cost-effective FBG inscription as well as dual wavelength operation.

Disclosures. The authors declare no conflicts of interest.

Data Availability. Data underlying the results presented in this paper are not publicly available at this time but may be obtained from the authors upon reasonable request.

REFERENCES

1. G. D. Marshall, R. J. Williams, N. Jovanovic, M. J. Steel, and M. J. Withford, "Point-by-point written fiber-Bragg gratings and their application in complex grating designs," Opt. Express **18**, 19844–19859 (2010).
2. Y. Zhang, C. Liao, C. Lin, Y. Shao, Y. Wang, and Y. Wang, "Surface plasmon resonance refractive index sensor based on fiber-interface waveguide inscribed by femtosecond laser," Opt. Lett. **44**, 2434–2437 (2019).
3. Q. Wang, H. Zhang, and D. N. Wang, "Cascaded multiple Fabry–Perot interferometers fabricated in no-core fiber with a waveguide for high-temperature sensing," Opt. Lett. **44**, 5145–5148 (2019).
4. T. Geernaert, K. Kalli, C. Koutsides, M. Komodromos, T. Nasilowski, W. Urbanczyk, J. Wojcik, F. Berghmans, and H. Thienpont, "Point-by-point fiber Bragg grating inscription in free-standing step-index and photonic crystal fibers using near-IR femtosecond laser," Opt. Lett. **35**, 1647–1649 (2010).
5. B. N. Chichkov, C. Momma, S. Nolte, F. von Alvensleben, and A. Tünnermann, "Femtosecond, picosecond and nanosecond laser ablation of solids," Appl. Phys. A **63**, 109–115 (1996).
6. X. Fang, C. R. Liao, and D. N. Wang, "Femtosecond laser fabricated fiber Bragg grating in microfiber for refractive index sensing," Opt. Lett. **35**, 1007–1009 (2010).
7. W. Cui, J. Si, T. Chen, and X. Hou, "Compact bending sensor based on a fiber Bragg grating in an abrupt biconical taper," Opt. Express **23**, 11031–11036 (2015).
8. Z. Chen, L. Yuan, G. Hefferman, and T. Wei, "Terahertz fiber Bragg grating for distributed sensing," IEEE Photon. Technol. Lett. **27**, 1084–1087 (2015).
9. X. Hu, D. Kinet, K. Chah, C.-F. J. Pun, H.-Y. Tam, and C. Caucheteur, "Bragg grating inscription in PMMA optical fibers using 400-nm femtosecond pulses," Opt. Lett. **42**, 2794–2797 (2017).
10. X. Cheng, D. S. Gunawardena, C.-F. J. Pun, J. Bonefacino, and H.-Y. Tam, "Single nanosecond-pulse production of polymeric fiber Bragg gratings for biomedical applications," Opt. Express **28**, 33573–33583 (2020).
11. G. Woyessa, H. K. Rasmussen, and O. Bang, "Zeonex—a route towards low loss humidity insensitive single-mode step-index polymer optical fibre," Opt. Fiber Technol. **57**, 102231 (2020).
12. R. Ishikawa, H. Lee, A. Lacraz, A. Theodosiou, K. Kalli, Y. Mizuno, and K. Nakamura, "Pressure dependence of fiber Bragg grating inscribed in perfluorinated polymer fiber," IEEE Photon. Technol. Lett. **29**, 2167–2170 (2017).
13. Y. Luo, Q. Zhang, H. Liu, and G.-D. Peng, "Gratings fabrication in benzildimethylketal doped photosensitive polymer optical fibers

using 355 nm nanosecond pulsed laser," Opt. Lett. **35**, 751–753 (2010).

14. J. Bonefacino, H.-Y. Tam, T. S. Glen, X. Cheng, C.-F. J. Pun, J. Wang, P.-H. Lee, M.-L. V. Tse, and S. T. Boles, "Ultra-fast polymer optical fibre Bragg grating inscription for medical devices," Light Sci. Appl. **7**, 17161 (2018).

15. W. Yuan, L. Khan, D. J. Webb, K. Kalli, H. K. Rasmussen, A. Stefani, and O. Bang, "Humidity insensitive TOPAS polymer fiber Bragg grating sensor," Opt. Express **19**, 19731–19739 (2011).

16. R. Min, B. Ortega, A. Leal-Junior, and C. Marques, "Fabrication and characterization of Bragg grating in CYTOP POF at 600-nm wavelength," IEEE Sens. Lett. **2**, 5000804 (2018).

17. I.-L. Bundalo, K. Nielsen, G. Woyessa, and O. Bang, "Long-term strain response of polymer optical fiber FBG sensors," Opt. Lett. **7**, 967–976 (2017).

18. A. Stefani, S. Andresen, W. Yuan, and O. Bang, "Dynamic characterization of polymer optical fibers," IEEE Sens. J. **12**, 3047–3053 (2012).

19. A. Lacraz, A. Theodosiou, and K. Kalli, "Femtosecond laser inscribed Bragg grating arrays in long lengths of polymer optical fibres; a route to practical sensing with POF," Electron. Lett. **52**, 1626–1627 (2016).

20. A. Leal-Junior, A. Frizera, M. J. Pontes, A. Fasano, G. Woyessa, O. Bang, and C. A. F. Marques, "Dynamic mechanical characterization with respect to temperature, humidity, frequency and strain in mPOFs made of different materials," Opt. Mater. Express **8**, 804–815 (2018).

21. J. N. Dash, X. Cheng, and H. Y. Tam, "Low gas pressure sensor based on polymer optical fiber grating," Opt. Lett. **46**, 933–936 (2021).

22. D. Sáez-Rodríguez, K. Nielsen, H. K. Rasmussen, O. Bang, and D. J. Webb, "Highly photosensitive polymethyl methacrylate microstructured polymer optical fiber with doped core," Opt. Lett. **38**, 3769–3772 (2013).

23. X. Hu, G. Woyessa, D. Kinet, J. Janting, K. Nielsen, O. Bang, and C. Caucheteur, "BDK-doped core microstructured PMMA optical fiber for effective Bragg grating photo-inscription," Opt. Lett. **42**, 2209–2212 (2017).

24. L. Pereira, R. Min, X. Hu, C. Caucheteur, O. Bang, B. Ortega, C. Marques, P. Antunes, and J. L. Pinto, "Polymer optical fiber Bragg grating inscription with a single Nd:YAG laser pulse," Opt. Express **26**, 18096–18104 (2018).

25. A. Fasano, G. Woyessa, P. Stajanca, C. Markos, A. Stefani, K. Nielsen, H. K. Rasmussen, K. Krebber, and O. Bang, "Fabrication and characterization of polycarbonate microstructured polymer optical fibers for high-temperature-resistant fiber Bragg grating strain sensors," Opt. Mater. Express **6**, 649–659 (2016).

26. G. Woyessa, A. Fasano, C. Markos, H. K. Rasmussen, and O. Bang, "Low loss polycarbonate polymer optical fiber for high temperature FBG humidity sensing," IEEE Photon. Technol. Lett. **29**, 575–578 (2017).

27. G. Emiliyanov, J. B. Jensen, P. E. Hoiby, L. H. Pedersen, E. M. Kjaer, L. Lindvold, and O. Bang, "Localized biosensing with TOPAS microstructured polymer optical fiber," Opt. Lett. **32**, 460–462 (2007).

28. G. Emiliyanov, P. E. Høiby, L. H. Pedersen, and O. Bang, "Selective serial multi-antibody biosensing with TOPAS microstructured polymer optical fibers," Sensors **13**, 3242–3251 (2013).

29. G. Woyessa, A. Fasano, C. Markos, A. Stefani, H. K. Rasmussen, and O. Bang, "ZEONEX microstructured polymer optical fiber: fabrication friendly fibers for high temperature and humidity insensitive Bragg grating sensing," Opt. Mater. Express **7**, 286–295 (2017).

30. G. Woyessa, J. K. M. Pedersen, A. Fasano, K. Nielsen, C. Markos, H. K. Rasmussen, and O. Bang, "ZEONEX-PMMA microstructured polymer optical FBGs for simultaneous humidity and temperature sensing," Opt. Lett. **42**, 1161–1164 (2017).

31. P. Akrami, A. I. Adamu, G. Woyessa, H. K. Rasmussen, O. Bang, and C. Markos, "All-polymer multimaterial optical fiber fabrication for high temperature applications," Opt. Mater. Express **11**, 345–354 (2021).

32. A. Lacraz, M. Polis, A. Theodosiou, C. Koutsides, and K. Kalli, "Femtosecond laser inscribed Bragg gratings in low loss CYTOP polymer optical fiber," IEEE Photon. Technol. Lett. **27**, 693–696 (2015).

33. G. Zhou, C. J. Pun, H. Tam, S. Member, A. C. L. Wong, C. Lu, and P. K. A. Wai, "Single-mode perfluorinated polymer optical fibers applications," IEEE Photon. Technol. Lett. **22**, 106–108 (2010).

34. G. Woyessa, A. Fasano, A. Stefani, C. Markos, K. Nielsen, H. K. Rasmussen, and O. Bang, "Single mode step-index polymer optical fiber for humidity insensitive high temperature fiber Bragg grating sensors," Opt. Express **24**, 1253–1260 (2016).

35. A. Leal-Junior, A. Theodosiou, A. Frizera-Neto, M. J. Pontes, E. Shafir, O. Palchik, N. Tal, S. Zilberman, G. Berkovic, P. Antunes, P. André, K. Kalli, and C. Marques, "Characterization of a new polymer optical fiber with enhanced sensing capabilities using a Bragg grating," Opt. Lett. **43**, 4799–4802 (2018).

36. A. Theodosiou, A. Lacraz, A. Stassis, C. Koutsides, M. Komodromos, and K. Kalli, "Plane-by-plane femtosecond laser inscription method for single-peak Bragg gratings in multimode CYTOP polymer optical fiber," J. Lightwave Technol. **35**, 5404–5410 (2017).

37. A. G. Leal, A. Frizera, A. Theodosiou, C. Díaz, M. Jimenez, R. Min, M. J. Pontes, K. Kalli, and C. Marques, "Plane-by-plane written, low-loss polymer optical fiber Bragg grating arrays for multiparameter sensing in a smart walker," IEEE Sens. J. **19**, 9221–9228 (2019).

38. J. Zhou, Z. Zhou, and D. Zhang, "Study on strain transfer characteristics of fiber Bragg grating sensors," J. Intell. Mater. Syst. Struct. **21**, 1117–1122 (2010).

39. H. P. Wang, P. Xiang, and X. Li, "Theoretical analysis on strain transfer error of FBG sensors attached on steel structures subjected to fatigue load," Strain **52**, 522–530 (2016).

40. C. D. Hussey and F. Martinez, "Approximate analytical forms for the propagation characteristics of single-mode optical fibres," Electron. Lett. **21**, 1103–1104 (1985).